

Article

Amine-Terminated Modified Succinic Acid-Magnetite Nanoparticles for Effective Removal of Malachite Green Dye from Aqueous Environment

Saad Melhi 

Department of Chemistry, College of Science, University of Bisha, Bisha 61922, Saudi Arabia; saadmehi@ub.edu.sa

Abstract: In this study, amine-terminated succinic acid-modified magnetic nanoparticles (MSA@TEPA) have been successfully synthesized using a facile two-step procedure as a new effective adsorbent for the removal of malachite green from aqueous solutions. The MSA@TEPA was characterized by scanning electron microscopy (SEM), Fourier-transform infrared spectroscopy (FTIR), zeta potential, thermal gravimetric analysis (TGA), and X-ray diffraction (XRD) analysis. The parameters influencing the adsorption capacity of MSA@TEPA, such as pH (3–8), contact time (t : 5–480 min), initial concentrations of MG dye (C_0 : 20–200 mg/L), and adsorbent mass (0.05–0.5 g), were evaluated. It was observed that, under specified experimental conditions (C_0 : 25 mg/L, pH: 7.1, T : 298 K, agitation rate: 100 rpm, and t : 420 min), the MSA@TEPA nanocomposite exhibits excellent adsorption efficiency (97.74%) for MG dye. The adsorption kinetics follow the PSO model, and the equilibrium data were fitted to the Langmuir isotherm with a maximum adsorption capacity of up to 282.65 mg/g. The thermodynamic parameters indicated that the adsorption process of MG dye was an exothermic process. After five consecutive cycles, MSA@TEPA nanocomposite still show good adsorption efficiency for MG dye. It is assumed that, because of the presence of amine group, adsorption mainly occurred through electrostatic interaction and H-bonding. In conclusion, the study shows a new and effective adsorbent with high adsorptive capacity, easy magnetic separation using an external magnetic field, and reusability for MG dye elimination from aqueous solutions.

Keywords: amine-terminated succinic acid; tetraethylenepentamine (TEPA); magnetic nanocomposite; malachite green (MG)



Citation: Melhi, S.

Amine-Terminated Modified Succinic Acid-Magnetite Nanoparticles for Effective Removal of Malachite Green Dye from Aqueous Environment. *Crystals* **2023**, *13*, 1301. <https://doi.org/10.3390/cryst13091301>

Academic Editors: Masayuki Nogami, Yong Yang, Nguyen Thi Viet Long and Nguyen Thi Nhat Hang

Received: 28 July 2023

Revised: 19 August 2023

Accepted: 22 August 2023

Published: 24 August 2023



Copyright: © 2023 by the author. Licensee MDPI, Basel, Switzerland. This article is an open access article distributed under the terms and conditions of the Creative Commons Attribution (CC BY) license (<https://creativecommons.org/licenses/by/4.0/>).

1. Introduction

Synthetic organic dyes are the most harmful water pollutants to the environment and human health because of their carcinogenic, mutagenic, and teratogenic behavior [1]. Different dyes are extensively used as colors in the paper, textile, leather, cosmetic, and plastic industries [2–4]. It is estimated that around 7×10^5 tons of dyestuff are manufactured each year and about 15% of the organic dyes are discharged into the aqueous environment, causing potential health hazards [3,5,6]. Malachite Green (MG, $C_{23}H_{25}N_2Cl$) is a cationic dye generally applied for coloring cotton, silk, leather, and paper products. It is also employed in aquaculture as a fungicide. By nature, MG is hazardous and toxic to human beings and other living organisms and its presence in a water environment causes damage to the liver, kidney, and respiratory system. Furthermore, it causes carcinogenic, mutagenic, and teratogenic effects on human cells [7–9]. Due to its noxious effects on living beings, it is therefore necessary to remove MG dye from wastewater.

Various physicochemical and biological techniques such as precipitation, membrane processes, coagulation, photocatalytic degradation, adsorption, chemical oxidation, ion exchange, and so on, have been applied for the elimination of dyes from contaminated water [10–12]. Amongst these, the adsorption technique has received significant attention

from researchers because it is promising, efficient, low-cost, eco-friendly, and economically viable for water treatment [11,13–15]. Various adsorbent materials, including polymers [16], zeolites [17], activated carbon [18], metal-organic frameworks (MOF) [19], mesoporous silica [20], high-availability sustainable biomass (rock melon skin (RMS) [21] and *Artocarpus odoratissimus* leaves [22]), and cellulosic biochar [23] have been used for the elimination of dyes from wastewater. But, owing to their small size, some of these adsorbents suffer from the difficulty of separating them from aqueous solutions. To solve this problem, separation using a magnetic nanoparticle adsorption technique has attracted a lot of attention due to its remarkable properties of being a rapid and effective method, its biocompatibility, high reusability, as well as its high efficiency after regeneration cycles [24]. For example, iron oxide (magnetite) nanoparticles, with a large specific surface area and high magnetic nature, can be used as an easy-to-isolate adsorbent from aqueous solutions via a magnet and are of good chemical stability [25]. However, magnetic nanoparticles have disadvantages, such as the fact that they are unstable under acidic conditions, oxidize in air, and aggregate due to the strong dipole–dipole magnetic attraction between nanoparticles. To overcome these problems, large numbers of compounds with magnetic natures and different functional groups have been developed. Various magnetic nanocomposites, such as cobalt ferrite silica magnetic nanocomposite [26], Fe_3O_4 @chitosan@ZIF-8 [27], magnetic biochar [28], poly(methyl methacrylate)/graphene oxide- Fe_3O_4 [28], $\text{MgO}/\text{Fe}_3\text{O}_4$ nanoparticles [29], and sodium alginate-coated Fe_3O_4 nanoparticles [30], were used to remove MG from aqueous solutions.

Succinic acid ($\text{C}_4\text{H}_6\text{O}_4$, SA) contains a dicarboxylic group that can serve as an active site for heavy metal ions adsorption [31,32]. The modification of magnetite nanoparticles using succinic acid (SA) leads to an improvement in the stability of magnetite nanoparticles and increases the pollutant's adsorption. Various amine-based sorbents, such as amino functionalized graphenes [33], polyaniline (PANI)–Nickel ferrite (NiFe_2O_4) [34], and 3-MPA@PMNPs [35], have been developed for the removal of MG dye from waste water. The presence of amine groups in the structure of magnetic nanocomposites provide the desired environment for the adsorption of metal ions [36], anionic metal species [37], and dyes [38]. Patil et al. prepared polyaniline–nickel ferrite magnetic nanocomposite as an adsorbent for the removal of MG dye from an aqueous solution. They found that the adsorption capacity was 4.09 mg/g at an optimum condition of 30 mg/L [34]. Hu et al. studied the abilities of Fe_3O_4 @ SiO_2 and Fe_3O_4 @ SiO_2 - NH_2 for the removal of MG dye and found that Fe_3O_4 @ SiO_2 - NH_2 showed a good removal efficiency of MG dye (90%) compared with Fe_3O_4 @ SiO_2 (60%) [39]. Tetraethylenepentamine (TEPA) is an organic polyamine molecule that contains five amino groups (two primary and three secondary functional groups) on its structure, which can serve as a binding site for metal ions [40], dyes [41], and CO_2 [42]. Ghasemi et al. used TEPFRCA and obtained the maximum adsorption of MG dye from the solvent phase. They reported a maximum adsorption capacity of 333.3 mg/g through the fast adsorption of MG dye from the solvent phase [43].

To the best of our knowledge, this was the first report of the design and synthesis of amine-terminated succinic acid-modified magnetic nanoparticles (MSA@TEPA) as an effective adsorbent using a facile two-step procedure. Firstly, magnetite nanoparticles functionalized with succinic acid were prepared using an in situ co-precipitation method and, next, were subsequently modified with tetraethylenepentamine (TEPA) via an amidation reaction. Then, the obtained MSA@TEPA product was characterized through SEM, FTIR, TGA, Zeta potential, and XRD analysis. The MSA@TEPA was used as an attractive adsorbent material for MG dye removal. The different parameters that influence adsorption processes, including, adsorbent dosage, initial MG concentration, solution pH, contact time, and temperature, were investigated. In addition, the adsorption nature was investigated through kinetic, isothermal, and thermodynamic parameters studies. Finally, this study provides a new effective magnetic nanocomposite as an adsorbent with high adsorptive capacity, easy magnetic separation using an external magnetic field, and reusability for MG dye removal from aqueous solutions

2. Materials and Methods

2.1. Materials

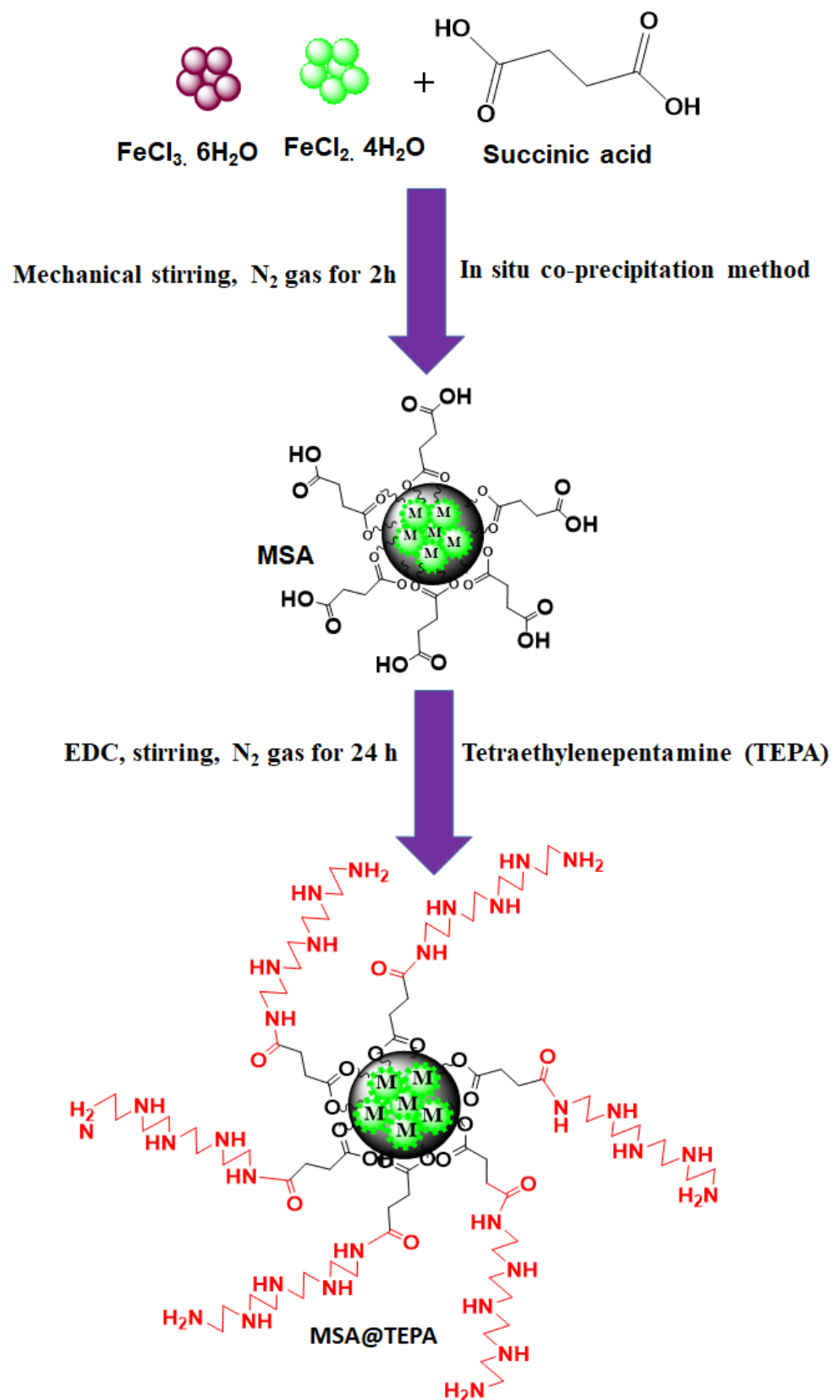
Tetraethylenepentamine ($C_8H_{23}N_5$, $\geq 97\%$), malachite green hydrochloride, ferric chloride ($FeCl_3 \cdot 6H_2O$), ferrous chloride ($FeCl_2 \cdot 4H_2O$), and 1-ethyl-3-(3 dimethylaminopropyl) carbodiimide (EDC) were purchased from Sigma–Aldrich, USA, India. Succinic anhydride ($C_4H_4O_3$, $\geq 99\%$) was purchased from Panreac, UK. Sodium hydroxide (NaOH, 97.5%), Nitric acid (HNO_3 , 69–71), Hydrochloric acid (HCl, 37%), and ammonium hydroxide (NH_4OH , 25%) were purchased from Merck, Germany.

2.2. Synthesis of Magnetic Nanocomposite (MSA@TEPA)

Magnetic nanocomposites (MSA@TEPA) were prepared via a facile two-step procedure involving preparing magnetic succinic acid (MSA) using an in situ co-precipitation method and its subsequent modification with high nitrogen content tetraethylenepentamine (TEPA). Firstly, the modified succinic acid magnetite nanoparticles were prepared as follows: 2.03 g of ferric salt and 0.746 g of ferrous salt were dissolved separately in deionized water (75 mL, 0.1 HCl) with a molar ratio of 2:1 under N_2 gas and magnetic stirring for 15 min, then the mixture was moved into a round bottom flask. After that, 0.5 g of succinic acid was added to the mixture of iron salts under nitrogen gas and magnetic stirring for 30 min, then the mixture was heated at 75 °C followed by the dropwise addition of NH_4OH (30 mL) under mechanical stirring for 2 h until the pH reached 10. After mechanical stirring for another 2 h, the black precipitate was separated using a magnet. The modified succinic acid magnetite nanoparticles formed were washed with deionized water (Scheme 1). Secondly, the obtained MSA nanocomposites were dispersed into a beaker containing 50 mL of ethanol, followed by 0.931 g of EDC addition to this solution under ultra-sonication for 40 min. After 40 min of stirring, 10 mL of TEPA was added dropwise into the MSA dispersion under magnetic stirring and nitrogen gas for 24 h. After the reaction completion, the obtained magnetic nanocomposites (MSA@TEPA) were collected through magnetic separation. Finally, the product was washed with de-ionized water and ethanol, and then dried at 60 °C for 24 h (Scheme 1).

2.3. Adsorption Experiments

The removal of MG dye from aqueous media by MSA@TEPA was studied through the batch elimination process. The different parameters that influence the efficiency of MG removal, including solution pH (3–8), contact time (t: 5–480 min), adsorbent mass (0.05–0.5 g), and initial concentrations of MG dye (C_0 : 20–200 mg/L), were studied. Generally, 20 mg of MSA@TEPA was added into an Erlenmeyer containing 20 mL of MG dye solution (25 mg/L). Then, the sample pH was adjusted up to ~ 7.1 by NaOH/HCl solution. Next, the sample was shaken at 100 rpm for the prescribed time (420 min) and then isolated using a magnet. The residual concentration of MG dye in the supernatant was determined using a UV–Vis spectrophotometer (Thermo Scientific, Evolution 600, Waltham, MA, USA) at the wavelength of 617 nm. The equilibrium removal efficiency of MG dye and the adsorption capacity (q_e mg/g) were calculated using Equations (1) and (2), respectively.



Scheme 1. Synthesis of MSA@TEPA.

$$R_e \% = \frac{C_o - C_e}{C_o} \times 100 \quad (1)$$

$$q_e = (C_o - C_e) \times \frac{V}{m} \quad (2)$$

where C_o and C_e (mg/L) represented the initial and final concentrations of MG dye, respectively, q_e (mg/g) is the adsorption capacity of MSA@TEPA toward MG dye, m (g) is the mass of MSA@TEPA, and V (L) is the MG solution volume.

3. Results

3.1. Characterization of MSA@TPEA

The FT-IR spectra of magnetite nanoparticles, TEPA, MSA, MSA@TPEA, and MG-loaded-MSA@TPEA, are displayed in Figure 1. The FT-IR spectra of MSA display broad bands at 3442, 2947, 2872, (1648, 1382 cm^{-1}) 1428, 1069, and 570 cm^{-1} that were assigned to hydroxyl (-OH), asymmetrical and symmetrical of C-H, carboxyl (COOH), C-O, and Fe-O bonds, respectively, indicating that the successful modification of succinic acid onto magnetite nanoparticles [44]. For TEPA, the characteristics bands at (3272 and 3349 cm^{-1}), 1451, and 1602 cm^{-1} were described as amino (NH_2) and C-N-C and N-H bonds onto the TEPA surface [45–47]. Compared with MSA, the band at 1632 cm^{-1} was described as the C=O stretching vibration of -CONH- formed in the MSA@TPEA product. In addition, the bands at 2855 and 2925 cm^{-1} (C-H stretching) became stronger in intensity, indicating the large numbers of -CH₂- introduced which proves that TEPA had been successfully bonded on the surface of MSA through the reaction between the carboxyl group of MSA and the amino group of TEPA [48,49]. The bands at 3435, 1483, 1260, 1057, and 570 cm^{-1} were assigned to the NH/OH, C-N-C bond, C-N, C-O, and Fe-O bonds. Based on these results, it is concluded that TEPA was grafted onto the MSA nanocomposite. After MG adsorption, the bands of functional groups decreased in their respective intensities. The bands at 3435, 1631, and 1265 cm^{-1} for ν (-OH/NH), -CONH-, and C-N were decreased in intensity and shifted to 3442, 1627, and 1251 cm^{-1} , respectively. Based on these results, it was concluded that MG dye was successfully adsorbed onto the MSA@TPEA surface.

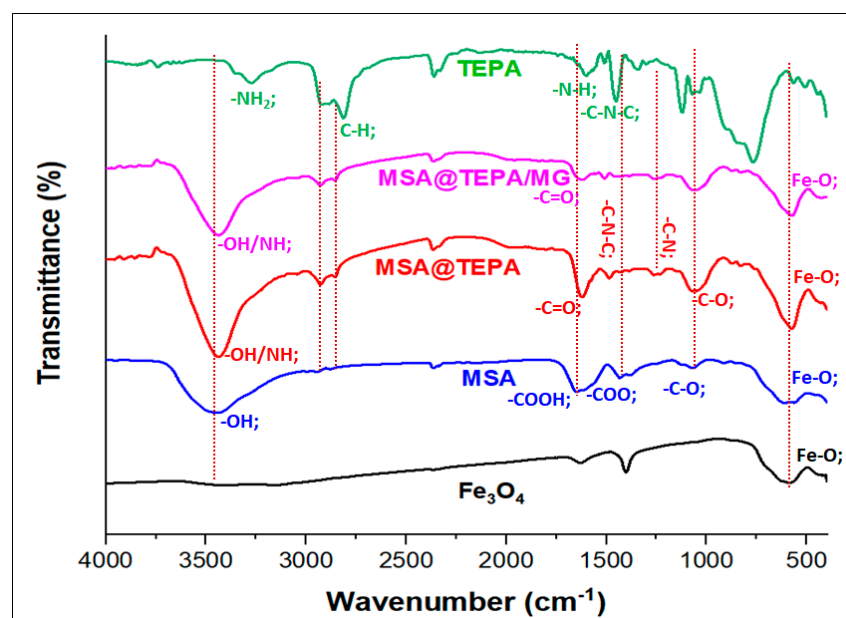


Figure 1. FT-IR spectra of Fe_3O_4 , TEPA, MSA, MSA@TPEA, and MG-loaded-MSA@TPEA.

The thermal stability curve of the prepared magnetite nanoparticles and MSA@TPEA nanocomposite is shown in Figure 2a. During the first step, the weight change in Fe_3O_4 and MSA@TPEA before 180 °C corresponds to the loss of moisture. The next two steps of weight loss up (15%) at 370 °C and (21.5%) at 750 °C were related to the decomposition of

the organic molecules (SA and TEPA) from the magnetite surface. The total weight loss of MSA@TEPA and pure magnetite nanoparticles was 41.5% and 9%, respectively. The overall TGA results indicate that the modified ratio of TEPA and SA onto magnetite nanoparticles is about 32.5%, which confirmed the formation of MSA@TEPA synthesis.

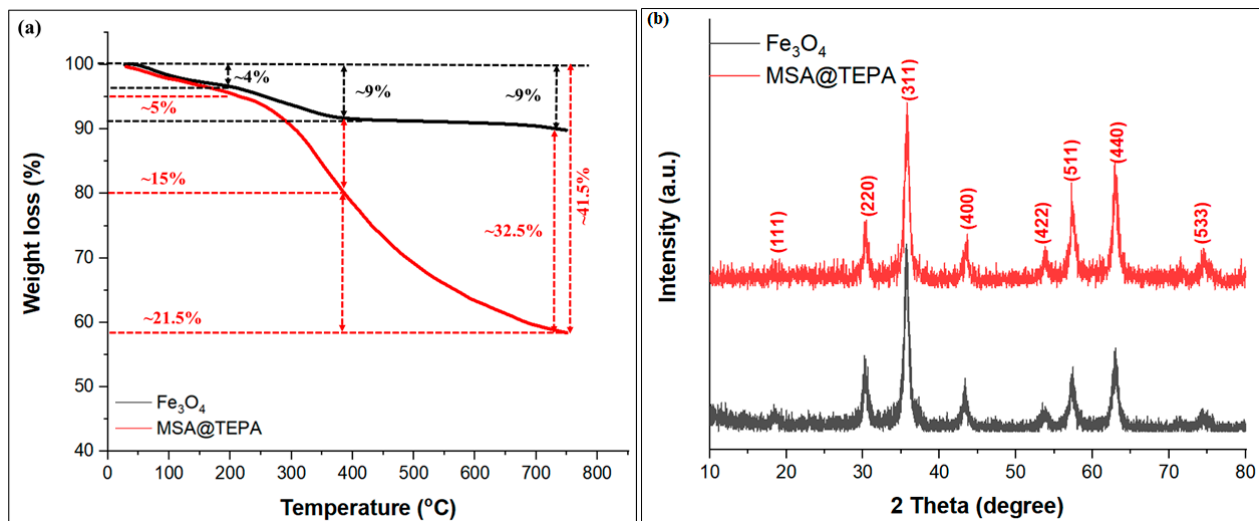


Figure 2. TGA curve (a) and (b) XRD pattern of the Fe₃O₄ nanoparticles and MSA@TEPA nanocomposite.

Figure 2b shows the XRD pattern of the Fe₃O₄ and MSA@TEPA nanocomposite. The diffraction patterns of both particles show eight peaks at $2\theta = 30.35^\circ, 35.71^\circ, 43.53^\circ, 53.82^\circ, 57.26^\circ, 62.86^\circ, \text{ and } 74.54^\circ$, corresponding to (220), (311) (400), (422), (511), (440), and (533), planes of cubic spinel Fe₃O₄. These results are in agreement with the magnetite's reflections (JCPDS file No. 019-0629) [50]. When compared with Fe₃O₄, the peaks of magnetite nanoparticles still exist in the XRD pattern of MSA@TEPA as well as the intensities of peaks in MSA@TEPA being almost the same as the pure magnetite nanoparticles, suggesting that the modification of magnetite with SA and TEPA did not change the phase of Fe₃O₄ nanoparticles [51]. The mean crystallite sizes (D) of Fe₃O₄ nanoparticles and MSA@TEPA nanocomposites were calculated using the Scherer equation:

$$D = \frac{k\lambda}{\beta \cos\theta} \quad (3)$$

where K is a constant (0.94), λ ($\lambda = 0.154 \text{ nm}$) is the X-ray wavelength, and β and θ are the line broadening at half-maximum intensity (FWHM) and the Bragg angle, respectively. The mean crystallite size for Fe₃O₄ nanoparticles and MSA@TEPA nanocomposite were 11.8 and 13.07 nm, respectively. The morphology of MSA@TEPA before and after MG dye adsorption is shown in Figure 3. It can be seen that, before adsorption, the MSA@TEPA has an irregular rough surface (Figure 3a,b) while, after MG dye adsorption, the surface of MSA@TEPA seems to be smooth, indicating the successful adsorption of MG dye on the MSA@TEPA surface (Figure 3c).

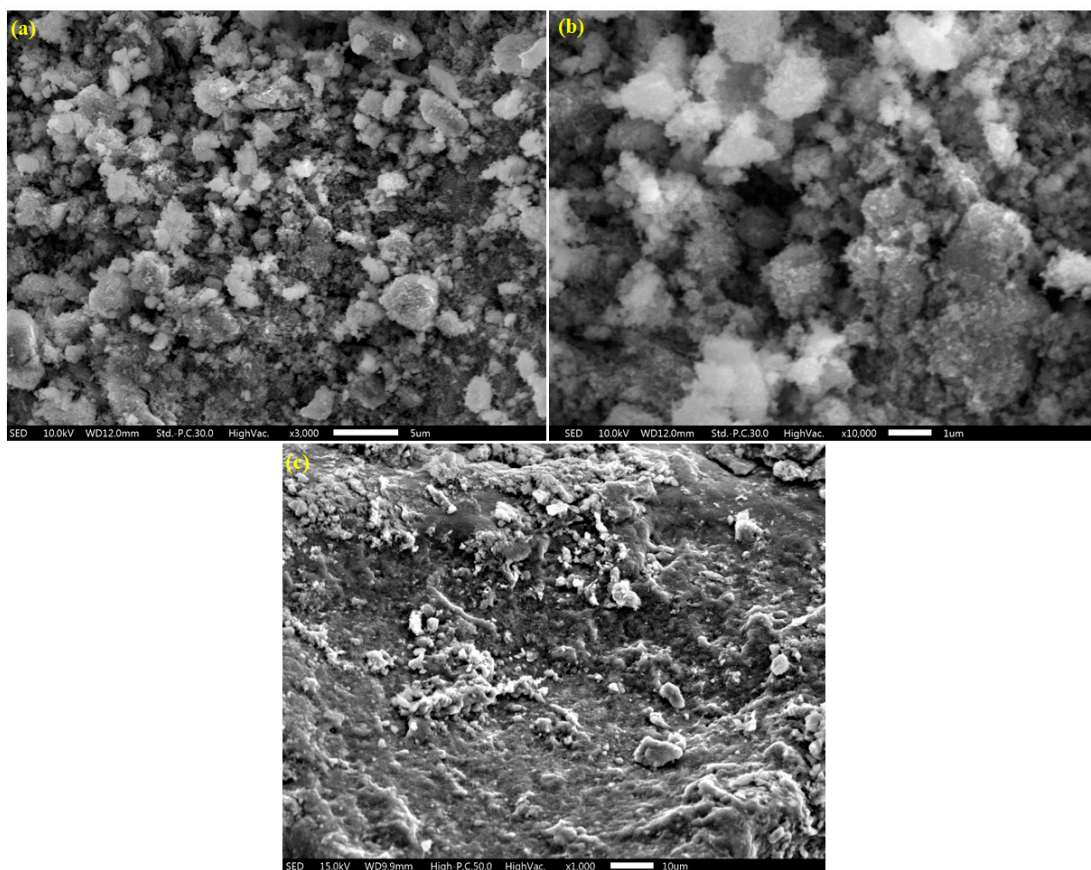


Figure 3. SEM image of MSA@TEPA at different magnification levels: (a) 50 μm , (b) 1 μm before and after MG dye adsorption (c).

3.2. Optimization of Adsorption Process Conditions

3.2.1. Effect of pH

It is known that the molecular structure of MG depends on the pH solution. In strongly basic conditions, the structure of malachite green converts to a carbinol base and loses its color owing to the reaction of OH with MG dye. Thus, the adsorption of MG by MSA@TEPA was investigated in the pH range from 3 to 8.1, as shown in Figure 4a. It can be seen that the efficiency of MG removal and adsorption capacity of MSA@TEPA was gradually increased from 28.82%, (9.01 mg/g) to 88.320%, (27.60 mg/g) with increasing solution pH from 3 to 6.1, respectively, and it reached a maximum value of 93.31%, (29.16 mg/g) at pH 7.1 [52]. The low MG removal at lower pH was assigned to the existence of protons (H^+) which might be because of the electrostatic repulsion between cationic MG ions and the protonated MSA@TEPA surface. On the other hand, with the pH increase, the positive charge of amine groups on the adsorbent surface decreases, thus, the electrostatic interactions with cationic MG^+ increase, which leads to an improvement in the efficiency of MG dye removal. The zeta potential results further support the pH results, as depicted in Figure 4a. It can be seen that the pH_{PZC} of MSA@TEPA was 6.7, indicating that the surfaces of MSA@TEPA are positively charged at $\text{pH} < \text{pH}_{\text{PZC}}$ and negatively charged at $\text{pH} > \text{pH}_{\text{PZC}}$. The different researchers also reported that low pH favors high adsorption, e.g., the MG adsorption on TiO_2 nanoparticles/anthracite [53] and reduced graphene oxide [54] reached a maximum value at $\text{pH} = 8$ and 8, respectively.

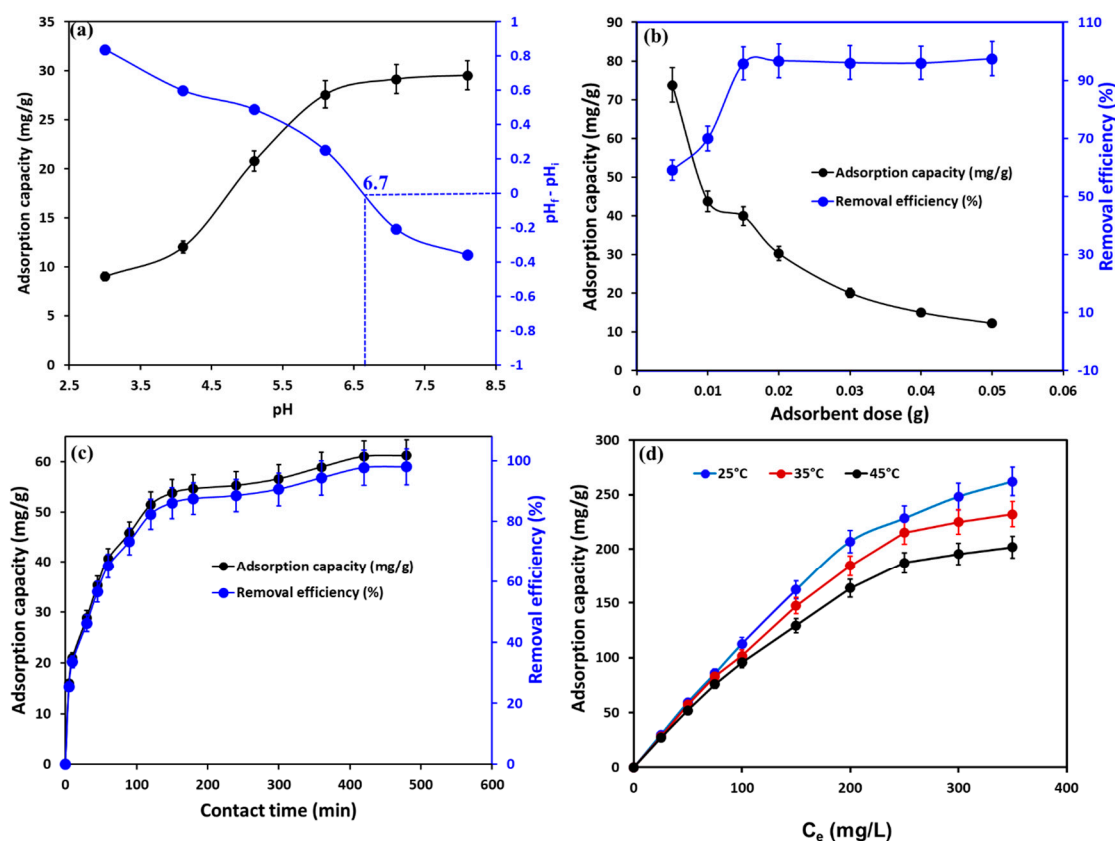


Figure 4. Effect of pH ([MG]: 25 mg/L; m: 0.02 g; T: 25 °C t: 24 h) (a), adsorbent dose ([MG]: 25 mg/L; t: 24 h; T: 25 °C) (b), contact time ([MG]: 25 mg/L; m: 0.02 g; T: 25 °C) (c), initial concentration of MG on the removal of MG dye onto MSA@TEPA ([MG]: 25 mg/L; m: 0.02 g; t: 420 min; T: 25 °C) (d).

3.2.2. Effect of Adsorbent Dosage

The influence of prepared MSA@TEPA mass on the efficiency of MG elimination was tested by varying the mass of MSA@TEPA between 0.005 and 0.05 g against a solution volume of 25 mL of 25 mg/L MG dye, as shown in Figure 4b. The efficiency of MG removal improved from 59.04% to 96.74% with an increase in the amount of MSA@TEPA nanocomposite from 0.005 to 0.02 g. Meanwhile, the adsorption capacity of MSA@TEPA toward MG reduces from 73.80 to 33.23 mg/g with the increasing amount of MSA@TEPA nanocomposite from 0.005 to 0.02 g. The reduction in the adsorption capacity of MSA@TEPA may be because of the aggregation of adsorption sites resulting in a decrease in the total adsorption surface area available for the MG dye [55]. Therefore, 0.02 g mass of adsorbent was selected as an optimum value for the rest of the experiments.

3.2.3. Effect of Contact Time

The influence of equilibrium time on the adsorption of MG onto MSA@TEPA was investigated at various shaking times in the range of 5 to 480 min. The time-dependence efficiency of MSA@TEPA for MG removal is given in Figure 4c. By increasing the time from 5 to 360 min, the MG removal and adsorption capacity efficiency gradually increases from 25.47% to 94.32%, respectively, then slowly decreases until it reaches an equilibrium at 360!min with maximum removal (97.74%) and adsorption capacity (61.09 mg/g). This might be due to the sufficient time interaction between the MSA@TEPA adsorbent and the MG dye molecules [56]. At 5 min, the MG dye removal efficiency was 25.47% while, at the equilibrium time of 30 min, this reached a maximum value of 46.19%. As already reported, the MG adsorption on the AC@ATPA composite [57] and Fe₃O₄@ATPA@AMPA [58] reached maximum adsorption capacity values of 14 mg/g and 58.9 mg/g at equilibration

times of 240 and 120 min, respectively. Thus, the optimum contact time was selected to be 420 min.

3.2.4. Effect of Initial Concentration and Temperature

The effect of MG concentration on the adsorption process was investigated at different initial concentrations between 20 and 200 mg/L under specific experimental conditions (m: 0.02 g; pH: 7.1; time: 420 min; T: 298 K; and agitation rate: 100 rpm), as displayed in Figure 4d. It can be seen that, with an increase in the initial concentration of MG dye from 25 to 350 mg/L, the MG removal efficiency decreases from 97.11% to 59.90%, while the adsorption capacity of MSA@TEPA toward MG dye increases from 29.72 to 262.06 mg/g. The increase in adsorption capacity with the increase in the initial MG concentration is because the higher the initial concentration of MG dye, the more collisions with active adsorption sites on the adsorbent surface, as well as the increase in the driving force of mass transfer leading to an increase in the adsorption capacity. At 25 mg/L, the MG dye removal efficiency was 97.11% while, at 100 mg/L, this reached the maximum value of 90.02%. The maximum adsorption capacity on the adsorbent was 262.06 mg/g at 25 °C. Figure 4d also reveals that, at higher temperatures, the sorption capacity is low. This means that the adsorption of MG dye on the adsorbent is an exothermic process.

3.3. Adsorption Modeling

3.3.1. Adsorption Isotherm

To better understand the maximum adsorption capacity of MSA@TEPA toward MG dye and also to study the mechanism of binding between MG dye and MSA@TEPA, different isotherm models, like the Langmuir [59], Freundlich [60], and Dubinin–Radushkevich (D-R) [61] isotherm models, were used. The nonlinear forms of these models are provided in Supplementary Information, Text S1. Table 1 gives a comparison between these isotherm models, and the obtained graph is shown in Figure 5a–c. The R^2 of Langmuir model ($R^2 = 0.99314$) is higher than that of the Freundlich ($R^2 = 0.96181$) and Dubinin–Radushkevich ($R^2 = 0.8876$) models, indicating that the MG adsorption onto MSA@TEPA follows the Langmuir isotherm model with q_e (282.65 mg/g). This indicates a monolayer homogenous adsorption of the MG molecules on the MSA@TEPA surface. All these results indicate that our prepared MSA@TEPA adsorbent showed good adsorption capacity for MG when compared with other various magnetic adsorbents like magnetic hydroxyapatite nanoparticles (208.06 mg/g) [62], MGO@Cellulose@Lipase (51.87 mg/g) [63], GO/Fe₃O₄ (96.9 mg/g) [64], and magnetic cobalt oxide nanoparticles (238.10 mg/g) [65].

Table 1. The values of parameters for each isotherm model.

Model	MG Dye		
	298 K	308 K	318 K
Langmuir			
q_m , mg/g	282.65	267.6503	240.50
K_L (L/mg)	0.071	0.042	0.029
R_L	0.360	0.487	0.579
R^2	0.99314	0.98715	0.99509
Freundlich			
K_f , (mg/g) (L/mg) ^{1/n}	51.51	36.39	26.11
n	2.91	2.62	2.46
R^2	0.96181	0.96088	0.96888
Dubinin–R			
q_s , mg/g	232.9	205.0	179.24
K_{D-R} (mol ² KJ ⁻²)	27.28	49.78	80.55
E (kJ mol ⁻¹)	0.135	0.100	0.053
R^2	0.8876	0.82899	0.87887

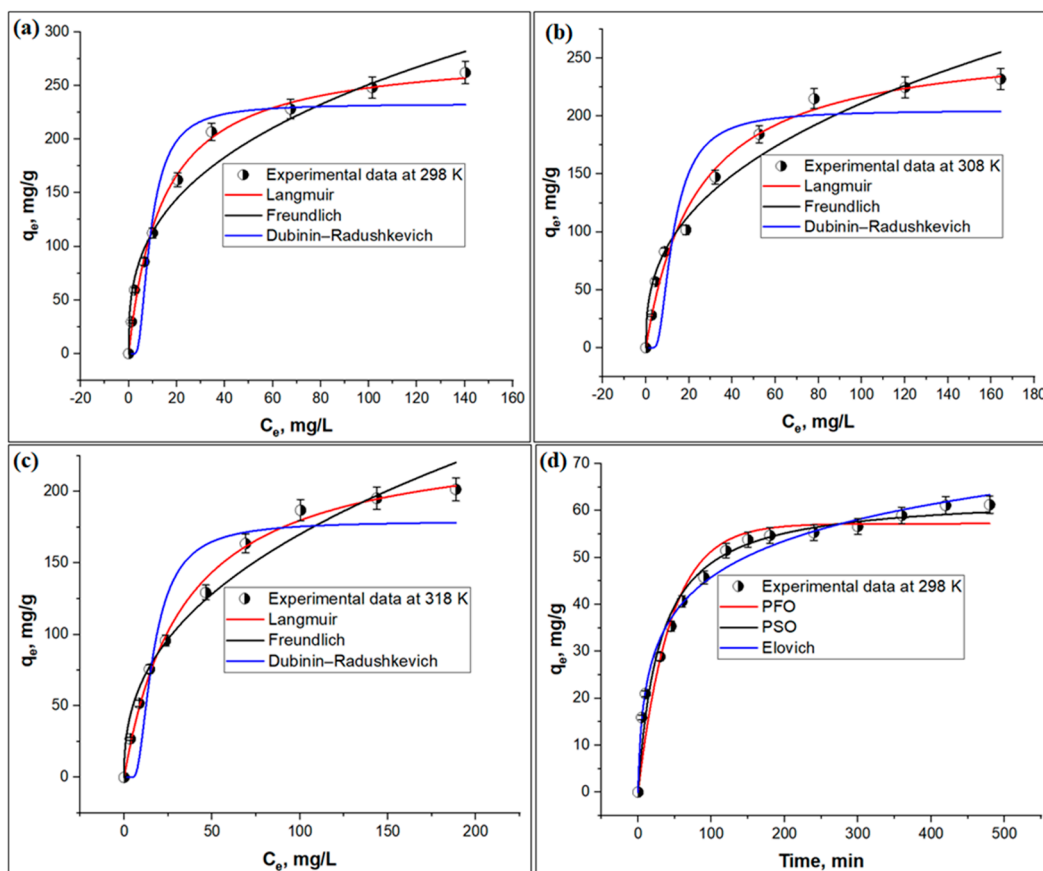


Figure 5. Experimental adsorption isotherms of MG adsorption on MSA@TPEA at 298 K (a), 308 K (b), and 318 K (c), and kinetic adsorption at 298 K (d).

3.3.2. Adsorption Kinetic

To understand the MG adsorption mechanism on the MSA@TEPA surface, the experimental data were assessed using nonlinear kinetic models like the pseudo-first-order (PFO) [66], pseudo-second-order (PSO), and Elovich models [67]. These kinetic parameter models are given in Supplementary Information, Text S2. The adsorption kinetic parameter values of MG dye onto the MSA@TEPA surface are illustrated in Table 2, and the obtained graph is shown in Figure 5d. The correlation coefficients for the PSO model ($R^2 = 0.9871$) are greater than that of the Elovich ($R^2 = 0.9731$) and PFO ($R^2 = 0.9448$) models, indicating that the MG adsorption follows the PSO kinetic model. Furthermore, the calculated $q_{e,exp.}$ (mg/g) value is close to the PSO model $q_{e,cal.}$ (mg/g) value, suggesting that the adsorption process seems to be a chemisorption process, which might result from the electrostatic attraction between the MG dye and the functional groups of the MSA@TEPA nanocomposite [68,69].

Table 2. The values of parameters for each kinetic model.

C_o (mg/L)	$q_{e,exp.}$ (mg/g)	Pseudo-First-Order			Pseudo-Second-Order			Elovich		
		$q_{e,cal.}$ (mg/g)	K_1 (1/min)	R^2	$q_{e2,cal.}$ (mg/g)	K_2 (g/mg-min)	R^2	A (mg/g min)	B (mg/g)	R^2
25	61.23	57.21	0.023	0.9448	63.36	0.00053	0.9871	6.42	0.089	0.9731

3.3.3. Adsorption Thermodynamics

The data obtained from the adsorption isotherm process were analyzed to assess the thermodynamic parameters, namely the standard entropy change (ΔS°), standard enthalpy change (ΔH°), and Gibbs energy (ΔG°). The following equations were used to calculate these parameters (4)–(6) [70]:

$$\Delta G^\circ = -RT \ln K_c \quad (4)$$

$$K_c = M.wt \times 1000 \times K_L \quad (5)$$

$$\ln K_c = \frac{\Delta S^\circ}{R} - \frac{\Delta H^\circ}{RT} \quad (6)$$

where K_L (L/g) is the Langmuir model constant, K_c referred to the adsorption equilibrium constant as calculated from Equation (4) [70], and $M.wt$ is the molecular weight of MG dye. The corresponding thermodynamic parameter values are listed in Table 3. The negative ΔG° values obtained for the adsorption of MG dye at all studied temperatures (298–318 K) indicate the spontaneity of the adsorption process. The negative ΔH° value (−34.76 (kJ/mol) suggests the exothermic nature of the adsorption process. Furthermore, the value of enthalpy changes also shed light on the type of adsorption mechanism, as for physisorption ($\Delta H^\circ < 20$ kJ/mol), for electrostatic interaction ($20 < \Delta H^\circ < 40$ kJ/mol), and for chemisorption ($80 < \Delta H^\circ < 450$ kJ/mol) [71]. As in our case, the value of ΔH° was −34.76 (kJ/mol), suggesting the electrostatic interaction of MG on the MSA@TEPA surface [71,72]. The negative values of ΔS° indicate a degree of disorder of the adsorbed MG at the solid/liquid interface, which is a normal and general phenomenon.

Table 3. Thermodynamic adsorption parameters for the adsorption of MG dye on MSA@TEPA.

ΔH° (kJ/mol)	ΔS° (J/mol.K)	ΔG° (kJ/mol)		
		298 K	308 K	318 K
−34.76	−32.29	−25.19	−24.71	−24.56

3.4. Proposed Adsorption Mechanism

After careful mathematical and experimental calculations, an adsorption mechanism of MG on MSA@TEPA was proposed, as shown in Figure 6. As MSA@TEPA has five amino groups on its surface, it might have an affinity to adsorb MG dye by electrostatic interaction and H-bonding. The FT-IR analysis has affirmed that MSA@TEPA adsorbent contains groups like amino, hydroxyl, and amide groups and, after MG adsorption on MSA@TEPA, the intensities of most of the FT-IR bands were reduced and shifted to lower wave numbers. For example, the bands at 3435, 1631, and 1265 cm^{-1} for $\nu(-\text{OH}/\text{NH})$, $-\text{CONH}-$, and C-N were decreased in intensity and shifted to 3442, 1627, and 1251 cm^{-1} , respectively, indicating that some sort of interaction (the H-bonding and electrostatic interaction) was involved during MG adsorption onto MSA@TPEA. This also confirms the successful MG adsorption onto MSA@TPEA surface. According to the pH results, as pH increases, the positive charge of amine groups on the adsorbent surface decreases. Thus, the chances of electrostatic interactions with cationic MG^+ increase, which lead to the MG dye removal efficiency. In conclusion, the interaction mechanism of MG onto the MSA@TEPA surface can be summarized as follows: (i) H-bonding between nitrogen of $\text{N}(\text{CH}_3)_2$ and $-\text{NH}$ groups on the MSA@TEPA surface and (ii) electrostatic attraction between positive charges of $^+\text{N}(\text{CH}_3)_2$ on the MG dye surface and negative charges of amino groups on the MSA@TEPA surface.

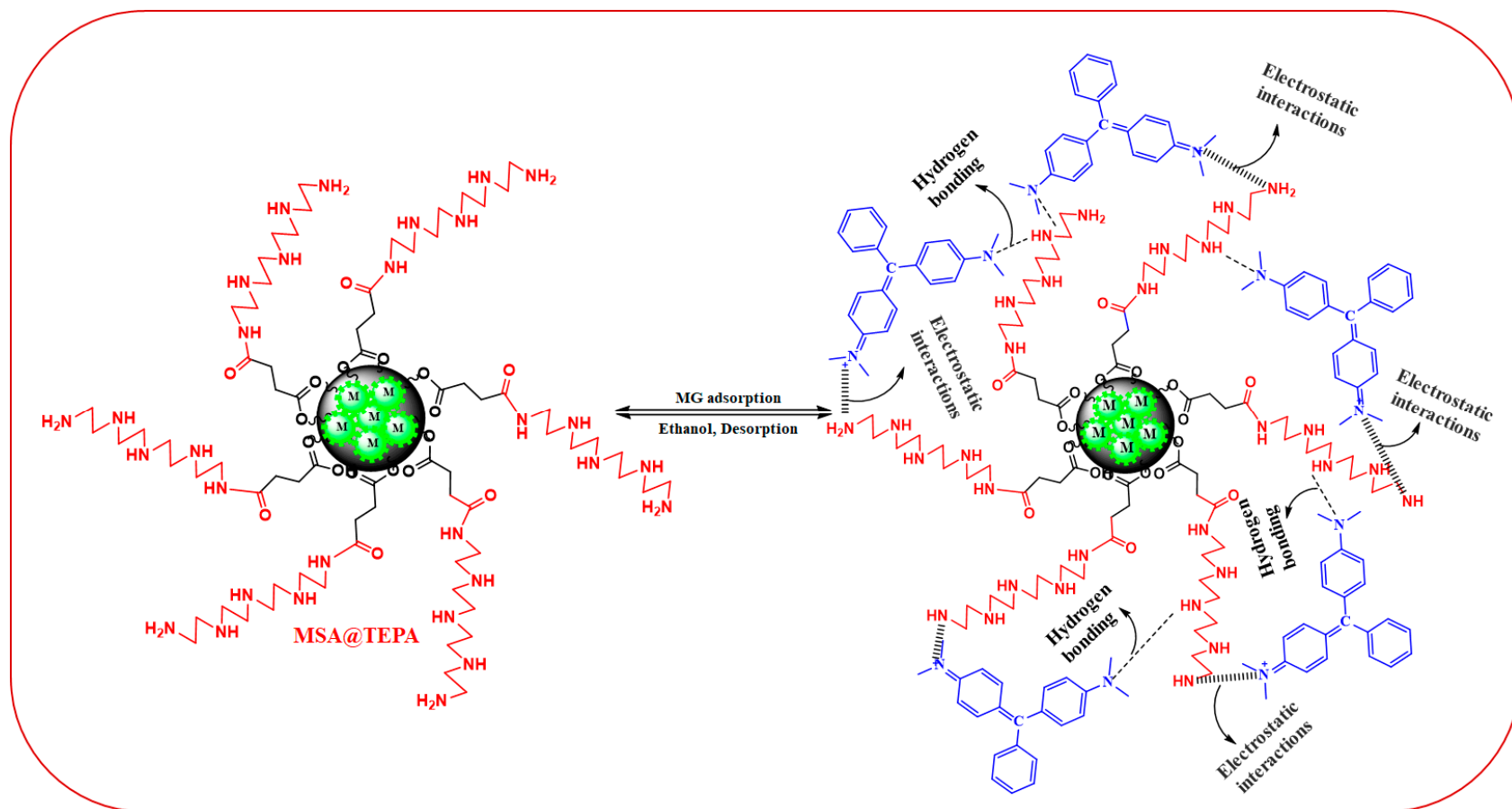


Figure 6. Proposed adsorption mechanism of MG onto MSA@TEPA.

3.5. Reusability of MSA@TEPA

To assess the reusability of MSA@TEPA nanocomposite, the removal of MG dye by MSA@TEPA was also tested over five consecutive cycles and with different eluents such as 0.01 M HCl, ethanol, and HCl/ethanol mixture. The results exhibited that the desorption efficiency was 32%, 73%, and 82% for HCl, ethanol, and HCl/ethanol mixture, respectively. Therefore, the eluent HCl/ethanol mixture was selected for subsequent experimental procedures. Figure 7 shows the reusability results of the MSA@TEPA nanocomposite. It was observed that the adsorption efficiency of MG was reduced to 61% after five consecutive adsorption–desorption cycles, which might be because of the depletion of adsorption active sites for MG and incomplete desorption of MG dye from MSA@TEPA.

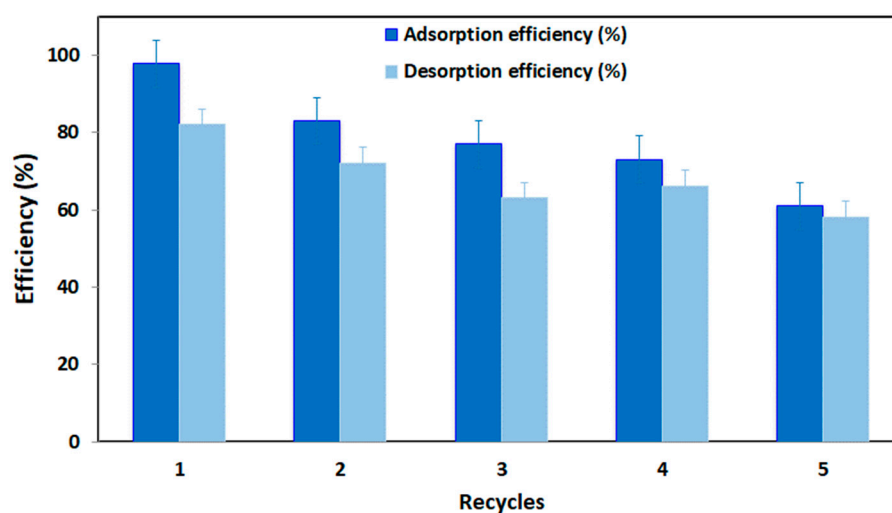


Figure 7. Adsorption–desorption cycle performance of MSA@TEPA for removal of MG dye.

4. Conclusions

In this study, amine-terminated modified succinic acid magnetite nanoparticles (MSA@TEPA) were prepared effectively using a simple, environmentally friendly coprecipitation method and were used as a new and efficient adsorbent for the elimination of malachite green from an aqueous medium. The removal of MG dye from aqueous media by MSA@TEPA was studied through the batch elimination process. MSA@TEPA were characterized using FTIR, XRD, and SEM techniques and the results showed successful modification of TEPA onto the MSA composite. MSA@TEPA exhibited good adsorption efficiency (97.74%) for MG under the specified experimental conditions (pH: 7.1, C_0 : 25 mg/L, T: 298 K, and t: 360 min). Such a good adsorption efficiency was attributed to the presence of poly amino groups in the structure of MSA@TEPA. The Langmuir isotherm and PSO kinetic models were applied and seemed to be the best-fitted models for the adsorption process. Furthermore, the thermodynamic parameters showed that the adsorption of MG ions onto MSA@TEPA was an exothermic process and occurred through electrostatic interaction and H-bonding. After five consecutive cycles, the material still shows good adsorption efficiency (61%) making it a highly reusable absorbent for MG dye. Finally, based on the above results and discussion, it can be concluded that MSA@TEPA can function as highly efficient adsorbents for MG removal, making the process cost-effective, environmentally friendly, and sustainable.

Supplementary Materials: The following supporting information can be downloaded at: <https://www.mdpi.com/article/10.3390/cryst13091301/s1>, Text S1: Adsorption isotherm, Text S2: Adsorption kinetics.

Funding: This research was funded by Deanship of Scientific Research at University of Bisha, Saudi Arabia through the Fast-Track Research Support Program.

Data Availability Statement: The data presented in this study are available on request from the author.

Acknowledgments: The author thanks the Deanship of Scientific Research at University of Bisha for supporting this work through the Fast-Track Research Support Program.

Conflicts of Interest: The author declare no conflict of interest.

References

1. Chakraborty, S.; Mukherjee, A.; Das, S.; Maddela, N.R.; Iram, S.; Das, P. Study on isotherm, kinetics, and thermodynamics of adsorption of crystal violet dye by calcium oxide modified fly ash. *Environ. Eng. Res.* **2021**, *26*, 190372. [[CrossRef](#)]
2. Alomar, T.S.; Al Masoud, N.; Sharma, G.; Al Othman, Z.A.; Naushad, M. Incorporation of trimetallic nanoparticles to the SiO₂ matrix for the removal of methylene blue dye from aqueous medium. *J. Mol. Liq.* **2021**, *336*, 116274. [[CrossRef](#)]
3. Naushad, M.; Alqadami, A.A.; Al-Kahtani, A.A.; Ahamad, T.; Awual, M.R.; Tatarchuk, T. Adsorption of textile dye using para-aminobenzoic acid modified activated carbon: Kinetic and equilibrium studies. *J. Mol. Liq.* **2019**, *296*, 112075. [[CrossRef](#)]
4. Faisal, A.A.H.; Shihab, A.H.; Naushad, M.; Ahamad, T.; Sharma, G.; Al-Sheetan, K.M. Green synthesis for novel sorbent of sand coated with (Ca/Al)-layered double hydroxide for the removal of toxic dye from aqueous environment. *J. Environ. Chem. Eng.* **2021**, *9*, 105342. [[CrossRef](#)]
5. Wang, K.; Wang, K.; Chen, Y.; Liang, S.; Guo, C.; Wang, W.; Wang, J. Adsorption-desorption behavior of malachite green by potassium permanganate pre-oxidation polyvinyl chloride microplastics. *Environ. Technol. Innov.* **2023**, *30*, 103138. [[CrossRef](#)]
6. Alqadami, A.A.; Naushad, M.; Al Othman, Z.A.; Ahamad, T. Adsorptive performance of MOF nanocomposite for methylene blue and malachite green dyes: Kinetics, isotherm and mechanism. *J. Environ. Manag.* **2018**, *223*, 29–36. [[CrossRef](#)] [[PubMed](#)]
7. Du, F.; Sun, L.; Huang, Z.; Chen, Z.; Xu, Z.; Ruan, G.; Zhao, C. Electrospun reduced graphene oxide/TiO₂/poly(acrylonitrile-co-maleic acid) composite nanofibers for efficient adsorption and photocatalytic removal of malachite green and leucomalachite green. *Chemosphere* **2020**, *239*, 124764. [[CrossRef](#)] [[PubMed](#)]
8. Ahmad, A.A.; Ahmad, M.A.; Yahaya, N.K.E.M.; Karim, J. Adsorption of malachite green by activated carbon derived from gasified Hevea brasiliensis root. *Arab. J. Chem.* **2021**, *14*, 103104. [[CrossRef](#)]
9. Gopinathan, R.; Kanhere, J.; Banerjee, J. Effect of malachite green toxicity on non target soil organisms. *Chemosphere* **2015**, *120*, 637–644. [[CrossRef](#)]
10. Alam, G.; Ihsanullah, I.; Naushad, M.; Sillanpää, M. Applications of artificial intelligence in water treatment for optimization and automation of adsorption processes: Recent advances and prospects. *Chem. Eng. J.* **2022**, *427*, 130011. [[CrossRef](#)]
11. Ahmed Alshareef, S.; Abdullah Alqadami, A.; Ali Khan, M.; Alanazi, H.S.; Raza Siddiqui, M.; Jeon, B.-H. Simultaneous co-hydrothermal carbonization and chemical activation of food wastes to develop hydrochar for aquatic environmental remediation. *Bioresour. Technol.* **2022**, *347*, 126363. [[CrossRef](#)] [[PubMed](#)]
12. Khan, M.A.; Alqadami, A.A.; Wabaidur, S.M.; Jeon, B.-H. Co-Carbonized Waste Polythene/Sugarcane Bagasse Nanocomposite for Aqueous Environmental Remediation Applications. *Nanomaterials* **2023**, *13*, 1193. [[CrossRef](#)] [[PubMed](#)]
13. Vo, T.S.; Hossain, M.M.; Lee, J.; Suhr, J.; Kim, K. Crosslinked 3D porous composite foams as adsorbents for efficient organic dye removal. *Environ. Technol. Innov.* **2023**, *29*, 102986. [[CrossRef](#)]
14. Ahmed, I.M.; Abd-Elhamid, A.I.; Aly, A.A.; Bräse, S.; Nayl, A.A. Synthesis of Ni-Fe-CO₃ layered double hydroxide as Effective Adsorbent to remove Cr(VI) and ARS-dye from aqueous media. *Environ. Technol. Innov.* **2023**, *31*, 103214. [[CrossRef](#)]
15. Majdoubi, H.; Alqadami, A.A.; Billah, R.E.; Otero, M.; Jeon, B.-H.; Hannache, H.; Tamraoui, Y.; Khan, M.A. Chitin-Based Magnesium Oxide Biocomposite for the Removal of Methyl Orange from Water. *Int. J. Environ. Res. Public Health* **2023**, *20*, 831. [[CrossRef](#)] [[PubMed](#)]
16. Şen, F.; Demirbaş, Ö.; Çalimli, M.H.; Aygün, A.; Alma, M.H.; Nas, M.S. The dye removal from aqueous solution using polymer composite films. *Appl. Water Sci.* **2018**, *8*, 206. [[CrossRef](#)]
17. Abukhadra, M.R.; Mohamed, A.S. Adsorption removal of safranin dye contaminants from water using various types of natural zeolite. *Silicon* **2019**, *11*, 1635–1647. [[CrossRef](#)]
18. Corda, N.C.; Kini, M.S. A review on adsorption of cationic dyes using activated carbon. In *Proceedings of the MATEC Web of Conferences*; EDP Sciences: Les Ulis, France, 2018; Volume 144, p. 2022. [[CrossRef](#)]
19. Nistor, M.A.; Muntean, S.G.; Maranescu, B.; Visa, A. Phosphonate metal-organic frameworks used as dye removal materials from wastewaters. *Appl. Organomet. Chem.* **2020**, *34*, e5939. [[CrossRef](#)]
20. Ekka, B.; Nayak, S.R.; Dash, P.; Patel, R.K. Removal of malachite green dye from aqueous solution using mesoporous silica synthesized from 1-octyl-3-methylimidazolium chloride ionic liquid. *AIP Conf. Proc.* **2016**, *1724*, 20011. [[CrossRef](#)]
21. Romzi, A.A.; Kooh, M.R.R.; Lim, L.B.L.; Priyantha, N.; Chan, C.M. Environmentally friendly adsorbent derived from rock melon skin for effective removal of toxic brilliant green dye: Linear versus non-linear analyses. *Int. J. Environ. Anal. Chem.* **2021**, *101*, 1–20. [[CrossRef](#)]
22. Mohamad Zaidi, N.A.H.; Sallehuddin, F.N.; Lim, L.B.L.; Kooh, M.R.R. Surface modification of Artocarpus odoratissimus leaves using NaOH, SDS and EDTA to enhance adsorption of toxic crystal violet dye. *Int. J. Environ. Anal. Chem.* **2023**, *103*, 1836–1854. [[CrossRef](#)]

23. Shaikh, W.A.; Kumar, A.; Chakraborty, S.; Naushad, M.; Islam, R.U.; Bhattacharya, T.; Datta, S. Removal of toxic dye from dye-laden wastewater using a new nanocomposite material: Isotherm, kinetics and adsorption mechanism. *Chemosphere* **2022**, *308*, 136413. [[CrossRef](#)] [[PubMed](#)]
24. Hotan Alsohaimi, I.; Alhumaimess, M.S.; Abdullah Alqadami, A.; Tharwi Alshammari, G.; Fawzy Al-Olaimi, R.; Abdeltawab, A.A.; El-Sayed, M.Y.; Hassan, H.M. Adsorptive performance of aminonaphthalenesulfonic acid modified magnetic-graphene oxide for methylene blue dye: Mechanism, isotherm and thermodynamic studies. *Inorg. Chem. Commun.* **2023**, *147*, 110261. [[CrossRef](#)]
25. Alqadami, A.A.; Naushad, M.; Abdalla, M.A.; Khan, M.R. Adsorptive Removal of Toxic Dye Using Fe₃O₄—TSC Nanocomposite: Equilibrium, Kinetic, and Thermodynamic Studies. *J. Chem. Eng. Data* **2016**, *61*, 3806–3813. [[CrossRef](#)]
26. Amiri, M.; Salavati-Niasari, M.; Akbari, A.; Gholami, T. Removal of malachite green (a toxic dye) from water by cobalt ferrite silica magnetic nanocomposite: Herbal and green sol-gel autocombustion synthesis. *Int. J. Hydrog. Energy* **2017**, *42*, 24846–24860. [[CrossRef](#)]
27. Zadvarzi, S.B.; Khavarpour, M.; Vahdat, S.M.; Baghbanian, S.M.; Rad, A.S. Synthesis of Fe₃O₄@chitosan@ZIF-8 towards removal of malachite green from aqueous solution: Theoretical and experimental studies. *Int. J. Biol. Macromol.* **2021**, *168*, 428–441. [[CrossRef](#)] [[PubMed](#)]
28. Burbano, A.A.; Gascó, G.; Horst, F.; Lassalle, V.; Méndez, A. Production, characteristics and use of magnetic biochar nanocomposites as sorbents. *Biomass Bioenergy* **2023**, *172*, 106772. [[CrossRef](#)]
29. Guo, F.; Jiang, X.; Li, X.; Jia, X.; Liang, S.; Qian, L. Synthesis of MgO/Fe₃O₄ nanoparticles embedded activated carbon from biomass for high-efficient adsorption of malachite green. *Mater. Chem. Phys.* **2020**, *240*, 122240. [[CrossRef](#)]
30. Mohammadi, A.; Daemi, H.; Barikani, M. Fast removal of malachite green dye using novel superparamagnetic sodium alginate-coated Fe₃O₄ nanoparticles. *Int. J. Biol. Macromol.* **2014**, *69*, 447. [[CrossRef](#)]
31. Karnitz, O.; Gurgel, L.V.A.; de Melo, J.C.P.; Botaro, V.R.; Melo, T.M.S.; de Freitas Gil, R.P.; Gil, L.F. Adsorption of heavy metal ion from aqueous single metal solution by chemically modified sugarcane bagasse. *Bioresour. Technol.* **2007**, *98*, 1291–1297. [[CrossRef](#)]
32. Gurgel, L.V.A.; Júnior, O.K.; Gil, R.P.d.F.; Gil, L.F. Adsorption of Cu(II), Cd(II), and Pb(II) from aqueous single metal solutions by cellulose and mercerized cellulose chemically modified with succinic anhydride. *Bioresour. Technol.* **2008**, *99*, 3077–3083. [[CrossRef](#)] [[PubMed](#)]
33. Guo, X.; Wei, Q.; Du, B.; Zhang, Y.; Xin, X.; Yan, L.; Yu, H. Removal of basic dyes (malachite green) from aqueous medium by adsorption onto amino functionalized graphenes in batch mode. *Desalin Water Treat.* **2015**, *53*, 818–825. [[CrossRef](#)]
34. Patil, M.R.; Shrivastava, V.S. Adsorption of malachite green by polyaniline–nickel ferrite magnetic nanocomposite: An isotherm and kinetic study. *Appl. Nanosci.* **2015**, *5*, 809–816. [[CrossRef](#)]
35. Ali, I.; Peng, C.; Ye, T.; Naz, I. Sorption of cationic malachite green dye on phyto-genic magnetic nanoparticles functionalized by 3-mercaptopropanoic acid. *RSC Adv.* **2018**, *8*, 8878–8897. [[CrossRef](#)] [[PubMed](#)]
36. Lin, C.-R.; Ivanova, O.S.; Petrov, D.A.; Sokolov, A.E.; Chen, Y.-Z.; Gerasimova, M.A.; Zharkov, S.M.; Tseng, Y.-T.; Shestakov, N.P.; Edelman, I.S. Amino-Functionalized Fe₃O₄@SiO₂ Core-Shell Magnetic Nanoparticles for Dye Adsorption. *Nanomaterials* **2021**, *11*, 2371. [[CrossRef](#)] [[PubMed](#)]
37. Niu, H.; Volesky, B. Characteristics of anionic metal species biosorption with waste crab shells. *Hydrometallurgy* **2003**, *71*, 209–215. [[CrossRef](#)]
38. Hozhabr Araghi, S.; Entezari, M.H. Amino-functionalized silica magnetite nanoparticles for the simultaneous removal of pollutants from aqueous solution. *Appl. Surf. Sci.* **2015**, *333*, 68–77. [[CrossRef](#)]
39. Sun, L.; Hu, S.; Sun, H.; Guo, H.; Zhu, H.; Liu, M.; Sun, H. Malachite green adsorption onto Fe₃O₄@SiO₂-NH₂: Isotherms, kinetic and process optimization. *RSC Adv.* **2015**, *5*, 11837–11844. [[CrossRef](#)]
40. Wang, K.; Zhang, F.; Xu, K.; Che, Y.; Qi, M.; Song, C. Modified magnetic chitosan materials for heavy metal adsorption: A review. *RSC Adv.* **2023**, *13*, 6713–6736. [[CrossRef](#)]
41. Zhao, D.; Zhang, L.; Lu, Y.; Li, H.; Wang, S.; Yuan, H.; Liu, X.; Wang, C.; Zhu, X.; Lu, J. Tetraethylenepentamine modified magnetic cellulose nanocrystal composites for removal of Congo red with high adsorption capacity. *J. Dispers. Sci. Technol.* **2022**, *43*, 1858–1871. [[CrossRef](#)]
42. Zhang, Q.; Dong, K.; Liu, Q.; Liu, Q.; Yao, J. Green and simple synthesis of poly (catechol-tetraethylenepentamine)@aminopropyl-modified silica composite for removing toxic Cr(VI). *J. Taiwan. Inst. Chem. Eng.* **2020**, *110*, 112–119. [[CrossRef](#)]
43. Ghasemi, M.; Mashhadi, S.; Asif, M.; Tyagi, I.; Agarwal, S.; Gupta, V.K. Microwave-assisted synthesis of tetraethylenepentamine functionalized activated carbon with high adsorption capacity for Malachite green dye. *J. Mol. Liq.* **2016**, *213*, 317–325. [[CrossRef](#)]
44. Saepudin, E.; Fadhilah, H.R.; Khalil, M. The influence of carboxylate moieties for efficient loading and pH-controlled release of doxorubicin in Fe₃O₄ magnetic nanoparticles. *Colloids Surf. A Physicochem. Eng. Asp.* **2020**, *602*, 125137. [[CrossRef](#)]
45. Alqadami, A.A.; Naushad, M.; Alothman, Z.A.; Ghfar, A.A. Novel Metal-Organic Framework (MOF) Based Composite Material for the Sequestration of U(VI) and Th(IV) Metal Ions from Aqueous Environment. *ACS Appl. Mater. Interfaces* **2017**, *9*, 36026–36037. [[CrossRef](#)] [[PubMed](#)]
46. Zhang, W.; Wang, H.; Hu, X.; Feng, H.; Xiong, W.; Guo, W.; Zhou, J.; Mosa, A.; Peng, Y. Multicavity triethylenetetramine-chitosan/alginate composite beads for enhanced Cr(VI) removal. *J. Clean. Prod.* **2019**, *231*, 733–745. [[CrossRef](#)]

47. Naushad, M.; Alqadami, A.A.; Ahamad, T. Removal of Cd(II) ion from aqueous environment using triaminotriethoxysilane grafted oxidized activated carbon synthesized via activation and subsequent silanization. *Environ. Technol. Innov.* **2020**, *18*, 100686. [[CrossRef](#)]
48. Wang, F.; Zhang, L.; Wang, Y.; Liu, X.; Rohani, S.; Lu, J. Fe₃O₄@SiO₂@CS-TETA functionalized graphene oxide for the adsorption of methylene blue (MB) and Cu(II). *Appl. Surf. Sci.* **2017**, *420*, 970–981. [[CrossRef](#)]
49. Cai, W.; Tan, L.; Yu, J.; Jaroniec, M.; Liu, X.; Cheng, B.; Verpoort, F. Synthesis of amino-functionalized mesoporous alumina with enhanced affinity towards Cr(VI) and CO₂. *Chem. Eng. J.* **2014**, *239*, 207–215. [[CrossRef](#)]
50. Krishna Murthy, T.P.; Gowrishankar, B.S.; Krishna, R.H.; Chandraprabha, M.N.; Mathew, B.B. Magnetic modification of coffee husk hydrochar for adsorptive removal of methylene blue: Isotherms, kinetics and thermodynamic studies. *Environ. Chem. Ecotoxicol.* **2020**, *2*, 205–212. [[CrossRef](#)]
51. Thangaraj, B.; Jia, Z.; Dai, L.; Liu, D.; Du, W. Lipase NS81006 immobilized on Fe₃O₄ magnetic nanoparticles for biodiesel production. *Ovidius Univ. Ann. Chem.* **2016**, *27*, 13–21. [[CrossRef](#)]
52. Li, Z.; Chen, K.; Chen, Z.; Li, W.; Biney, B.W.; Guo, A.; Liu, D. Removal of malachite green dye from aqueous solution by adsorbents derived from polyurethane plastic waste. *J. Environ. Chem. Eng.* **2021**, *9*, 104704. [[CrossRef](#)]
53. Ramadan, H.S.; Ali, R.A.M.; Mobarak, M.; Badawi, M.; Selim, A.Q.; Mohamed, E.A.; Bonilla-Petriciolet, A.; Seliem, M.K. One-step fabrication of a new outstanding rutile TiO₂ nanoparticles /anthracite adsorbent: Modeling and physicochemical interpretations for malachite green removal. *Chem. Eng. J.* **2021**, *426*, 131890. [[CrossRef](#)]
54. Rout, D.R.; Jena, H.M. Removal of malachite green dye from aqueous solution using reduced graphene oxide as an adsorbent. *Mater. Today Proc.* **2021**, *47*, 1173–1182. [[CrossRef](#)]
55. Geng, Y.; Zhang, J.; Zhou, J.; Lei, J. Study on adsorption of methylene blue by a novel composite material of TiO₂ and alum sludge. *RSC Adv.* **2018**, *8*, 32799–32807. [[CrossRef](#)]
56. Sahraei, R.; Hemmati, K.; Ghaemy, M. Adsorptive removal of toxic metals and cationic dyes by magnetic adsorbent based on functionalized graphene oxide from water. *RSC Adv.* **2016**, *6*, 72487–72499. [[CrossRef](#)]
57. Aldawsari, A.M.; Alshaimi, I.H.; Al-Kahtani, A.A.; Alqadami, A.A.; Ali Abdalla, Z.E.; Saleh, E.A.M. Adsorptive performance of aminoterephthalic acid modified oxidized activated carbon for malachite green dye: Mechanism, kinetic and thermodynamic studies. *Sep. Sci. Technol.* **2021**, *56*, 835–846. [[CrossRef](#)]
58. Melhi, S.; Algamdi, M.; Alqadami, A.A.; Khan, M.A.; Alosaimi, E.H. Fabrication of magnetically recyclable nanocomposite as an effective adsorbent for the removal of malachite green from water. *Chem. Eng. Res. Des.* **2022**, *177*, 843–854. [[CrossRef](#)]
59. Wallis, A.; Dollard, M.F. Local and global factors in work stress—The Australian dairy farming exemplar. *Scand. J. Work Environ. Health Suppl.* **2008**, *34*, 66–74.
60. Über die Adsorption in Lösungen. *Z. Phys. Chem.* **1907**, *57U*, 385. [[CrossRef](#)]
61. Dubinin, M.M. The Equation of the Characteristic Curve of Activated Charcoal Proceedings of the Academy of Sciences. *Phys. Chem. Sect.* **1947**, *55*, 331.
62. Hua, Y.; Xu, D.; Liu, Z.; Zhou, J.; Han, J.; Lin, Z.; Xu, D.; Chen, G.; Huang, X.; Chen, J.; et al. Effective adsorption and removal of malachite green and Pb²⁺ from aqueous samples and fruit juices by pollen-inspired magnetic hydroxyapatite nanoparticles/hydrogel beads. *J. Clean. Prod.* **2023**, *411*, 137233. [[CrossRef](#)]
63. Mahmoud, M.E.; El-Sharkawy, R.M.; Ibrahim, G.A.A. A novel bionanocomposite from doped lipase enzyme into magnetic graphene oxide-immobilized-cellulose for efficient removal of methylene blue and malachite green dyes. *J. Mol. Liq.* **2022**, *368*, 120676. [[CrossRef](#)]
64. Li, W.; Xu, M.; Cao, Q.; Luo, J.; Yang, S.; Zhao, G. Magnetic GO/Fe₃O₄ for rapid malachite green (MG) removal from aqueous solutions: A reversible adsorption. *RSC Adv.* **2021**, *11*, 19387–19394. [[CrossRef](#)] [[PubMed](#)]
65. Mohanta, J.; Dey, B.; Dey, S. Magnetic Cobalt Oxide Nanoparticles: Sucrose-Assisted Self-Sustained Combustion Synthesis, Characterization, and Efficient Removal of Malachite Green from Water. *J. Chem. Eng. Data* **2020**, *65*, 2819–2829. [[CrossRef](#)]
66. Lagergren, S. About the theory of so-called adsorption of soluble substances. *Handlingar* **1898**, *24*, 1–39.
67. Chien, S.H.; Clayton, W.R. The catalytic oxidation of carbon monoxide on manganese dioxide. *Sci. Soc. Am. J.* **1980**, *44*, 265–268. [[CrossRef](#)]
68. Jayasanth Kumari, H.; Krishnamoorthy, P.; Arumugam, T.K.; Radhakrishnan, S.; Vasudevan, D. An efficient removal of crystal violet dye from waste water by adsorption onto TLAC/Chitosan composite: A novel low cost adsorbent. *Int. J. Biol. Macromol.* **2017**, *96*, 324–333. [[CrossRef](#)]
69. Mirza, A.; Ahmad, R. An efficient sequestration of toxic crystal violet dye from aqueous solution by Alginate/Pectin nanocomposite: A novel and ecofriendly adsorbent. *Groundw. Sustain. Dev.* **2020**, *11*, 100373. [[CrossRef](#)]
70. Lima, E.C.; Hosseini-Bandegharaei, A.; Moreno-Piraján, J.C.; Anastopoulos, I. A critical review of the estimation of the thermodynamic parameters on adsorption equilibria. Wrong use of equilibrium constant in the Van't Hoof equation for calculation of thermodynamic parameters of adsorption. *J. Mol. Liq.* **2019**, *273*, 425–434. [[CrossRef](#)]

71. Machado, F.M.; Bergmann, C.P.; Fernandes, T.H.M.; Lima, E.C.; Royer, B.; Calvete, T.; Fagan, S.B. Adsorption of Reactive Red M-2BE dye from water solutions by multi-walled carbon nanotubes and activated carbon. *J. Hazard. Mater.* **2011**, *192*, 1122–1131. [[CrossRef](#)]
72. Erwa, I.Y.; Ishag, O.A.; Alrefaei, O.A.; Hassan, I.M. Nonlinear Fitting for Estimation of Adsorption Equilibrium, Kinetic and Thermodynamic Parameters of Methylene Blue onto Activated Carbon. *J. Turk. Chem. Soc. Sect. A Chem.* **2022**, *9*, 67–84. [[CrossRef](#)]

Disclaimer/Publisher's Note: The statements, opinions and data contained in all publications are solely those of the individual author(s) and contributor(s) and not of MDPI and/or the editor(s). MDPI and/or the editor(s) disclaim responsibility for any injury to people or property resulting from any ideas, methods, instructions or products referred to in the content.